Journal of Power Sources 195 (2010) 6463–6467

Contents lists available at ScienceDirect

Journal of Power Sources

journal homepage: www.elsevier.com/locate/jpowsour

Short communication

Electrocatalytic activity of perovskite $La_{1-x}Sr_xMnO_3$ towards hydrogen peroxide reduction in alkaline medium

Guiling Wang, Yanyan Bao, Yongmei Tian, Jing Xia, Dianxue Cao*

College of Material Science and Chemical Engineering, Harbin Engineering University, Nantong St. #145, Harbin 150001, PR China

ARTICLE INFO

Article history:
Received 24 March 2010
Received in revised form 18 April 2010
Accepted 19 April 2010
Available online 24 April 2010

Keywords:
Lanthanum strontium manganate
Perovskite
Hydrogen peroxide electroreduction
Alkaline electrolytes
Metal semi-fuel cell

ABSTRACT

Perovskite-type series of compounds $La_{1-x}Sr_xMnO_3$ are synthesized by a sol–gel method using Chitosan as the gelling agent. Their catalytic activity for hydrogen peroxide electroreduction in 3.0 mol dm^{-3} KOH at room temperature is evaluated by means of cyclic voltammetry and chronoamperometry. Effects of annealing temperature and the ratio of La to Sr of $La_{1-x}Sr_xMnO_3$ on their catalytic performance are investigated. Among this series of compounds, $La_{0.4}Sr_{0.6}MnO_3$ calcined at 650 °C exhibits the highest activity, which is comparable with Co_3O_4. An aluminum–hydrogen peroxide semi-fuel cell using $La_{0.4}Sr_{0.6}MnO_3$ as cathode catalyst achieves a peak power density of 170 mW cm^{-2} at 170 mA cm^{-2} and 1.0 V running on 0.6 mol dm^{-3} H_2O_2.

1. Introduction

Fuel cells are attractive power sources for space and underwater applications because of their high energy density. When working in the air-free environment, fuel cells generally require pure oxygen (liquid or compressed) as oxidant. The bulky tank for carrying oxygen significantly reduces the energy density and safety standard of fuel cell systems. H_2O_2 has been investigated as an alternative oxidant in replacing of oxygen because H_2O_2 is liquid, its handling and storage are easier. In addition, the electroreduction kinetics of H_2O_2 is faster than that of oxygen. Therefore, fuel cells with H_2O_2 oxidant tend to have high performance and are more compact comparing with those using oxygen as oxidant. Several types of fuel cells using H_2O_2 as oxidant have been investigated, including direct borohydride–hydrogen peroxide fuel cell [1–7], metal–hydrogen peroxide semi-fuel cell [8–17], hydrazine–hydrogen peroxide fuel cell [18], direct methanol–hydrogen peroxide fuel cell [19,20], and biofuel–hydrogen peroxide fuel cell [21,22].

Several types of electrocatalysts for hydrogen peroxide reduction have been investigated, including: (1) noble metals, such as platinum, palladium, iridium, gold, silver and a combination of these [7,10–12,14,16,17,23]; (2) macrocycle complexes of transition metals, such as Fe– and Co–porphyrin, Cu–triazine complexes [24–26]; (3) transition metal oxides, such as cobalt oxides [15,27]. Noble metal catalysts usually show high activity for H_2O_2 electroreduction, but they significantly catalyze the chemical decomposition of H_2O_2 to oxygen, leading to the reduction of H_2O_2 utilization. Besides, they are expensive. In a recent study, we demonstrated that cheap transition metal oxides (e.g., Co_3O_4) exhibit superior activity and stability for H_2O_2 electroreduction in alkaline medium [15]. The chemical decomposition of H_2O_2 on Co_3O_4 can be minimized by using low concentration of H_2O_2 [27].

Perovskite-type materials, particularly of $La_{1-x}Sr_xMnO_3$(LSM), as potential cathode of high temperature solid oxide fuel cells have been extensively investigated [28]. LSM possess mixed ionic–electronic conductivity, which is highly beneficial for LSM being used as cathodes in fuel cells. Very recently, the electrocatalytic behavior of LSM towards oxygen reduction in an ambient temperature alkaline electrolyte has been reported [29,30]. It was found that, within $La_{1-x}Sr_xMnO_3$ series, $La_{0.4}Sr_{0.6}MnO_3$ exhibits the greatest catalytic activity and the greatest proportion of direct four-electron oxygen reduction compared to two-electron reduction. Even though $La_{0.4}Sr_{0.6}MnO_3$ has around 0.15 V greater overpotential than Pt for oxygen reduction in alkaline medium at room temperature, its relative low cost makes it a promising cathode to replace precious platinum for low temperature alkaline fuel cells [29]. Besides, $La_{0.4}Sr_{0.6}MnO_3$ cathode is insensitive to the presence of organic fuels such as ethylene glycol [30]. In this paper, the electrocatalytic activity and stability of $La_{1-x}Sr_xMnO_3$ for hydrogen peroxide reduction in alkaline medium were investigated. The performance of $La_{0.4}Sr_{0.6}MnO_3$ as the cathode catalyst of an alkaline aluminum–hydrogen peroxide semi-fuel cell was evaluated.

* Corresponding author. Tel.: +86 451 82589036; fax: +86 451 82589036.
E-mail address: caodianxue@hrbeu.edu.cn (D. Cao).

0378-7753/$ – see front matter © 2010 Elsevier B.V. All rights reserved.
doi:10.1016/j.jpowsour.2010.04.061

2. Experimental

2.1. Preparation and characterization of $La_{1-x}Sr_xMnO_3$

$La_{1-x}Sr_xMnO_3$ powders were synthesized by a sol–gel method using $La(NO_3)_3{\cdot}6H_2O$, $Sr(NO_3)_2$ and $Mn(NO_3)_3$ as source materials and Chitosan as the gelling agent. An appropriate amount of $La(NO_3)_3{\cdot}6H_2O$, $Sr(NO_3)_2$ and $Mn(NO_3)_3$ was weighed out and dissolved in a small amount of ultra-pure water (Milli-Q), respectively. The nitrate solutions were then added to a Chitosan solution, which was prepared by dissolving appropriate amount of Chitosan in 2% (volume fraction) acetic acid. The resulting solution was stirred vigorously whilst being heated to 80 °C and held at this temperature until water was nearly completely removed and a homogeneous transparent solution was obtained. The solution was then slowly cooled down to ambient temperature to form a gel, which was dried at 100 °C for 12 h in an oven to obtain a dry gel. The dry gel was grounded to fine powders and calcined at temperatures between 550 and 750 °C for 5 h in air. After cooling down to room temperature, the powder was grounded again and sieved by passing through a 400 mesh sieve. The fine powders below 400 mesh were used for material characterization and electrode preparation. The structure of the samples was analyzed using X-ray diffractometer (Rigaku TTR III) with Cu Kα radiation (λ = 0.1514178 nm). The 2θ ranges from 10° to 90° with a scan rate of 5° min^{-1} and a step width of 0.01°. The morphology was examined by scanning electron microscope equipped with an energy-dispersive X-ray spectrometer (SEM/EDX, JEOL JSM-6480). Thermo-gravimetric and differential thermal analysis (TG/DTA) was performed with a Pyris-Diamond thermal analyzer (Perkin-Elmer) in a flow of air (40 cm^3 min^{-1}) at a heating rate of 20 °C min^{-1} from room temperature up to 800 °C in an Al_2O_3 sample pan.

2.2. Preparation of $La_{1-x}Sr_xMnO_3$ electrode

To prepare $La_{1-x}Sr_xMnO_3$ electrodes, $La_{1-x}Sr_xMnO_3$ powder and carbon black (Vulcan XC-72) were dispersed in anhydrous ethanol by sonication for 10 min to obtain a suspension, to which a PTFE emulsion was added. The mixture was sonicated for another 15 min and then heated at 80 °C in a water bath until a thick paste was formed. The paste was smeared on a nickel foam current collector, heated at 110 °C for 12 h and then pressed under 10 MPa pressure. The obtained electrodes consists of 80 wt.% $La_{1-x}Sr_xMnO_3$, 8 wt.% carbon black and 12 wt.% PTFE.

2.3. Electrochemical measurements

Electrochemical measurements were performed in a standard three-electrode electrochemical cell with saturated Ag/AgCl reference electrode and glassy carbon rod counter electrode. The electrolyte was 3.0 mol dm^{-3} KOH containing different concentrations of H_2O_2. The $La_{1-x}Sr_xMnO_3$ working electrode has a dimension of 10 mm × 10 mm × 0.5 mm and a $La_{1-x}Sr_xMnO_3$ loading of 20 mg cm^{-2}. Cyclic voltammetry and chronoamperometry were conducted using a computerized VMP3/Z potentiostat (Biologic) controlled by the EC-lab software. The reported current densities were calculated using the geometrical area of the electrode. All solutions were made with analytical grade chemical reagents and ultra-pure water (Milli-Q, 18 ΩM cm). All potentials were referred to the saturated Ag/AgCl, KCl reference electrode.

2.4. Al–H_2O_2 semi-fuel cell tests

The performance of $La_{0.4}Sr_{0.6}MnO_3$ as cathode catalyst of the Al–H_2O_2 semi-fuel cell was examined using a home-made flow through test cell made of Plexiglas. Both the aluminum alloy anode (LF6, 91.9% Al, 6.5% Mg, 0.6% Mn, 0.3% Fe, 0.3% Si, 0.2% Zn, 0.1% Ti) and the $La_{0.6}Sr_{0.4}MnO_3$ cathode have the same geometrical area of 4.0 cm^2 (20 mm × 20 mm). Nafion-115 (DuPont) membrane was used to separate the anode and the cathode compartments. The anolyte (3.0 mol dm^{-3} KOH) and the catholyte (3.0 mol dm^{-3} KOH + 0.6 mol dm^{-3} H_2O_2) were pumped into the bottom of the anode and the cathode compartment, respectively, using an individual peristaltic pump, at a flow rate of 80 cm^3 min^{-1}, and exited at the top of the compartments. The performance of the Al–H_2O_2 was recorded at ambient temperature using a computer-controlled E-load system (Arbin).

3. Results and discussion

3.1. Characterization of $La_{1-x}Sr_xMnO_3$

The decomposition behavior and phase evolution of the $La_{0.6}Sr_{0.4}MnO_3$ dry gel were investigated by TG–DTA. Fig. 1 shows the TG–DTA curves of $La_{0.6}Sr_{0.4}MnO_3$ dry gel measured from room temperature to 800 °C in air flow. As can be seen from the TG curve, the weight loss of the dry gel takes place roughly in four stages noted by stage I, II, III and IV on the graph. Domain I (around 23–130 °C) corresponding to a weight loss of 3.5% is a consequence of the removal of the residual adsorbed and hydrated water. Domain II (around 130–330 °C) associating to a weight loss of 41% is due to the loss of nitrate and acetic anions by decomposition and oxidation. Four weak exothermal peaks at 177, 216, 280, and 319 °C in the DTA curve (insert of Fig. 1) likely relate to the various decomposition stages of the anions. Domain III (around 330–420 °C) with a weight loss of 30% is accompanied by strong sharp exothermal peaks at 415 °C and can be assigned to the combustion of Chitosan gelling agent because the decomposition of Chitosan starts at around 320 °C [31]. No significant weight loss is observed in Domain IV (around 420–800 °C) which implies that almost all the nitrite anion and organic derivatives are removed. The weak exothermic peak at 625 °C is most probably due to formation of the perovskite phase.

XRD analysis was conducted to obtain information about the formation of crystallographic phase during thermal treatment. Fig. 2 shows the XRD patterns of the $La_{0.6}Sr_{0.4}MnO_3$ powders annealed at 550, 600, 650 and 700 °C. The standard crystallographic spectrum of perovskite $La_{0.65}Sr_{0.35}MnO_3$ from JCPDS card No. 50-0308 was included for comparison. For the sample calcined at 550 °C, a few peaks corresponding to perovskite phase $La_{0.6}Sr_{0.4}MnO_3$ were observed but not well developed. The samples calcined above 600 °C displayed the typical pattern of perovskite $La_{0.6}Sr_{0.4}MnO_3$ and the corresponding characteristic peaks became sharper as the

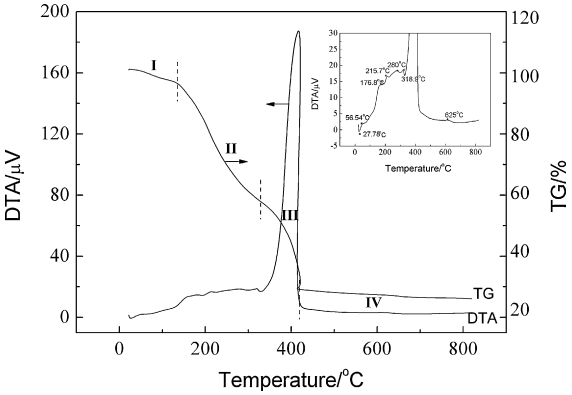

Fig. 1. TG–DTA curves of $La_{0.6}Sr_{0.4}MnO_3$.

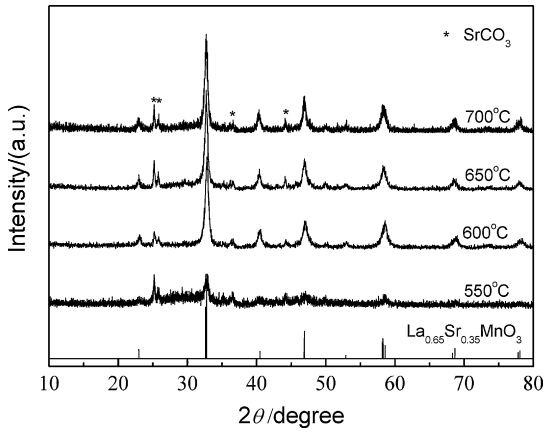

Fig. 2. XRD patterns of $La_{0.6}Sr_{0.4}MnO_3$ calcined at different temperatures.

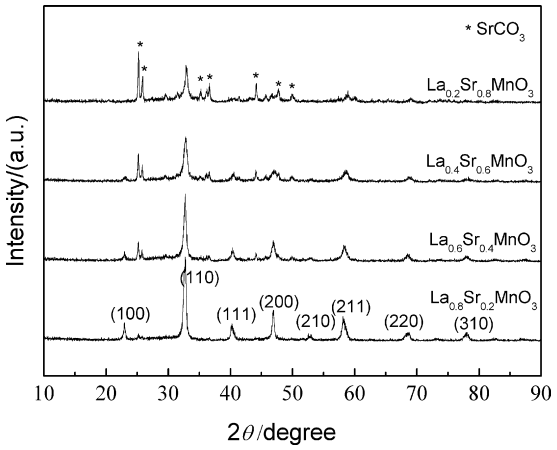

Fig. 4. XRD patterns of $La_{1-x}Sr_xMnO_3$ with x equal to 0.2, 0.4, 0.6 and 0.8.

calcination temperature elevates, demonstrating that better crystalline structure was formed. The average crystallite size of the calcined samples was estimated from XRD patterns using Scherrer equation [29,32] and values are between 18 and 22 nm. Peak about 25°, 36° and 44° can be attributed to $SrCO_3$, which likely results from the reaction of Sr^{2+} with CO_2 (from the combustion of Chitosan or air) during the annealing process. No peaks from impurities such as manganese oxides, lanthanum oxides and strontium oxides were observed. The morphology of $La_{0.6}Sr_{0.4}MnO_3$ sample calcined at 650 °C is shown in Fig. 3. Most of the particles are in irregular shape with a small portion having the rod-like shape. The atomic ratio of the transition metals in the sample was determined by EDX to be 0.62:0.38:1.0 (La:Sr:Mn).

The influence of the ratio of La to Sr on the structure of $La_{1-x}Sr_xMnO_3$ compounds was investigated by XRD. Fig. 4 shows the XRD patterns of a series of $La_{1-x}Sr_xMnO_3$ compounds with x from 0.2 to 0.8. The samples were calcined at 650 °C. The XRD patterns are in good agreement with that reported in literatures for perovskite-type $La_{1-x}Sr_xMnO_3$ [29,33] except peaks from $SrCO_3$ were observed in this study. With the increase of the ratio of Sr to La, the intensity of peaks from $SrCO_3$ increases implying that some Sr^{2+} are not incorporated in the crystal phase of $La_{1-x}Sr_xMnO_3$. The average crystallite size of $L_{1-x}Sr_xMnO_3$ estimated using Scherrer equation is about 21, 23, 18, and 39 nm for x = 0.2, 0.4, 0.6, and 0.8, respectively.

3.2. Electrocatalytic performance of $La_{1-x}Sr_xMnO_3$ for H_2O_2 reduction

Fig. 5 shows the influence of thermal treatment temperature on the electrocatalytic performance of $La_{0.6}Sr_{0.4}MnO_3$. The cyclic voltammograms were recorded in 3 mol dm^{-3} KOH containing 0.6 mol dm^{-3} H_2O_2 at a scan rate of 5 mV s^{-1}. It can be seen that the onset potential for H_2O_2 reduction was around −0.15 V and is independent of the calcination temperature. The differential of current density to applied potential (dj/dE) increased with the calcination temperature from 550 to 650 °C and then decreased with the further increase of the temperature to 700 °C, which demonstrates that the sample calcined at 650 °C exhibited the highest electrocatalytic performance. This is likely because the sample calcined at 650 °C achieved a better balance between crystal structure and specific surface area as indicated by TG–DTA and XRD results. Lower thermal treatment temperature favors larger specific surface area but worsens crystallinity. Higher calcination temperature leads to better crystallinity but smaller specific surface area duo to the sintering.

Fig. 6 shows the effect of the ratio of La to Sr on the electrocatalytic performance of $La_{1-x}Sr_xMnO_3$. The cyclic voltammograms were recorded in 3.0 mol dm^{-3} KOH containing 0.6 mol dm^{-3} H_2O_2 at a scan rate of 5 mV s^{-1}. The CV demonstrates that H_2O_2 electroreduction starts at around −0.15 V, which is around −0.05 V more negative than that for spinel Co_3O_4 we reported previously [15]. This onset potential is nearly independent of the composition of $La_{1-x}Sr_xMnO_3$. However the current density varies obviously with

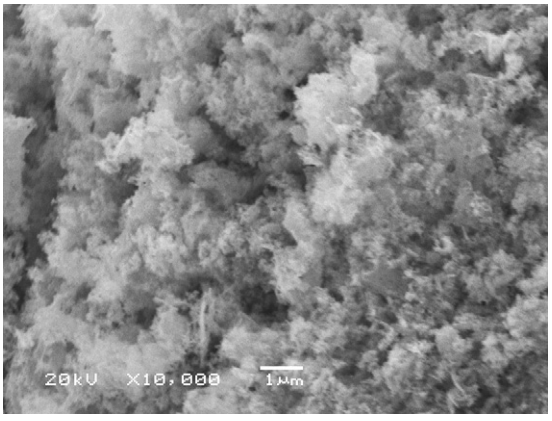

Fig. 3. SEM image of $La_{0.6}Sr_{0.4}MnO_3$ powder calcined at 650 °C.

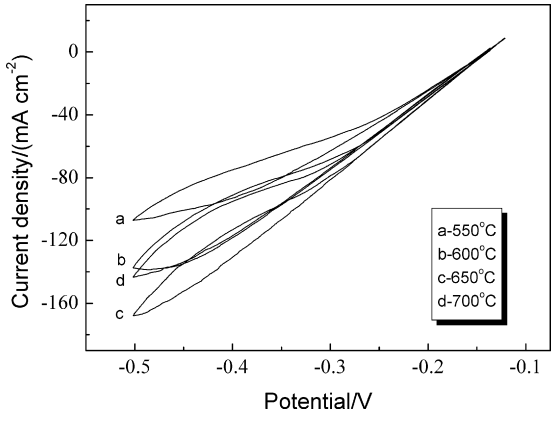

Fig. 5. Cyclic voltammograms of $La_{0.6}Sr_{0.4}MnO_3$ calcined at different temperatures taken in 3.0 mol dm^{-3} KOH containing 0.6 mol dm^{-3} H_2O_2. Scan rate: 5 mV s^{-1}.

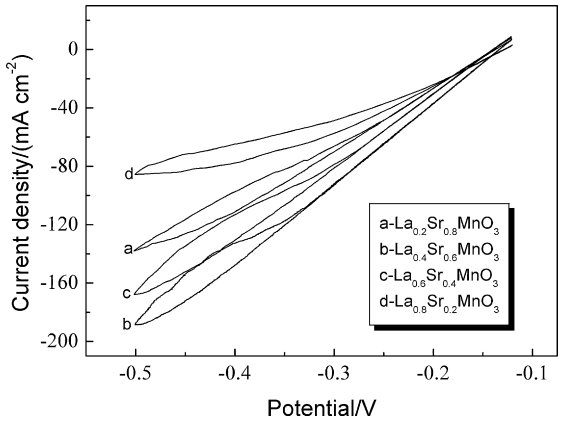

Fig. 6. Cyclic voltammograms of $La_{1-x}Sr_xMnO_3$ recorded in 3.0 mol dm^{-3} KOH containing 0.6 mol dm^{-3} H_2O_2. Scan rate: 5 mV s^{-1}.

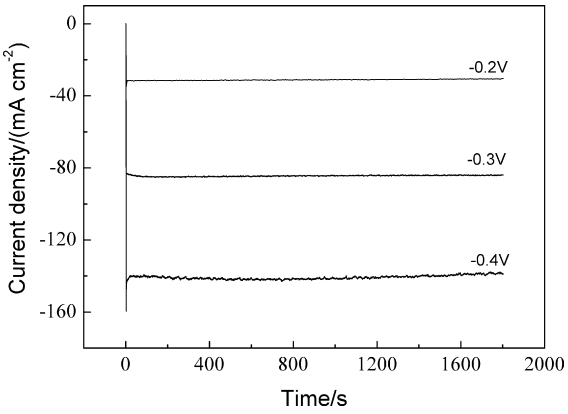

Fig. 8. Chronoamperometric curves for H_2O_2 electroreduction on $La_{0.4}Sr_{0.6}MnO_3$ electrode at different potentials in 3.0 mol dm^{-3} KOH + 0.6 mol dm^{-3} H_2O_2.

the mole ration of La to Sr, for example, the current density at −0.4 V is −78, −130, −145 and −110 mA cm^{-2} with x = 0.2, 0.4, 0.6, and 0.8, respectively. Obviously, $La_{0.4}Sr_{0.6}MnO_3$ exhibits the best catalytic performance for H_2O_2 electroreduction in alkaline medium. Similarly, Donne et al. recently reported that among the series of compounds $La_{1-x}Sr_xMnO_3$ (where x = 0, 0.2, 0.4, 0.6, 0.8 and 1.0), it is $La_{0.4}Sr_{0.6}MnO_3$ that shows the highest catalytic activity towards oxygen electroreduction in an ambient temperature KOH electrolyte.

Fig. 7 shows the influence of H_2O_2 concentration on the electroreduction performance of $La_{0.4}Sr_{0.6}MnO_3$ electrode. It can be seen that the dj/dE remains constant but the cathodic peak current density remarkably increased with the increase of H_2O_2 concentration. The cathodic peak current density displayed an approximate linear relationship with the H_2O_2 concentration, implying that the reduction reaction at the peak potential was controlled by H_2O_2 diffusion. The nearly linear behavior of the polarization curves in the cathodic scan suggests a large ohmic resistive effect of the electrode, which is likely due to the low conductivity of $La_{0.4}Sr_{0.6}MnO_3$ at room temperature. Even though higher limiting current density can be achieved at higher H_2O_2 concentration, the chemical decomposition of H_2O_2 to O_2 becomes more significant at high H_2O_2 concentration as indicated by the formation of gas bubbles on the electrode surface. No gas bubbles were observed at H_2O_2 concentrations below 0.4 mol dm^{-3}, but obvious gas evolution occurred when H_2O_2 concentration exceeds 0.6 mol dm^{-3}. Using low concentration H_2O_2 is essential for keeping high H_2O_2 utilization efficiency. The $La_{0.4}Sr_{0.6}MnO_3$ exhibits a comparable activity to Co_3O_4 nanoparticles. For example, the mass current density measured at −0.4 V for 0.6 mol dm^{-3} H_2O_2 is 7.3 mA mg^{-1} for $La_{0.4}Sr_{0.6}MnO_3$ and 8 mA mg^{-1} for Co_3O_4 powder. Perovskite-type compounds possess mixed ionic and electronic conductivity, which has been found to be highly beneficial for them acting as electrocatalysts for fuel cells. Their catalytic activity, ionic and electronic conductivity can be tuned by changing the elements in both A-site (such as La and Sr) and B-site (such as Mn, Co, Ni, Fe and Cu). This study demonstrated that perovskite $La_{1-x}Sr_xMnO_3$ displays considerable catalytic activity and stability towards electroreduction of H_2O_2 in alkaline medium at room temperature, which opens up the possibility for the development of perovskite-type compounds as H_2O_2 cathode. By changing the composition of the compounds, better catalytic performance might be achieved. Further investigation is undergoing in this Lab.

The stability of $La_{0.4}Sr_{0.6}MnO_3$ electrode for H_2O_2 electroreduction was investigated by chronoamperometric measurements. Fig. 8 shows chronoamperometric curves of H_2O_2 electroreduction on $La_{0.4}Sr_{0.6}MnO_3$ calcined at 650 °C. At the mixed kinetic-diffusion control potentials (−0.2 and −0.3 V), currents reached to steady-state after a few seconds and displayed no sign of decrease within 30 min test period, indicating that $La_{0.4}Sr_{0.6}MnO_3$ has a good stability for catalyzing hydrogen peroxide electroreduction. At the near diffusion control potential (−0.4 V), currents decreased slightly after around 1000 s. This behavior likely resulted from the depletion of H_2O_2 near the electrode surface.

The performance of $La_{0.4}Sr_{0.6}MnO_3$ as the cathode catalyst of Al–H_2O_2 semi-fuel cell was investigated. Fig. 9 shows plots of cell

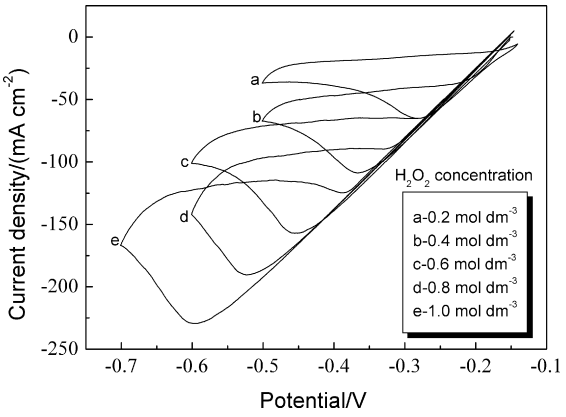

Fig. 7. Cyclic voltammograms of $La_{0.4}Sr_{0.6}MnO_3$ measured in 3.0 mol dm^{-3} KOH containing H_2O_2 with different concentrations between 0.2 and 1.0 mol dm^{-3}. Scan rate: 5 mV s^{-1}.

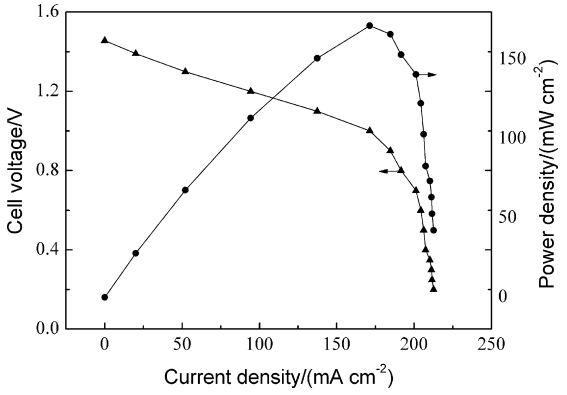

Fig. 9. Performance of Al–H_2O_2 single semi-fuel cell with $La_{0.4}Sr_{0.6}MnO_3$ cathode. Anolyte: 3.0 mol dm^{-3} KOH at a flow rate of 80 cm^3 min^{-1}. Catholyte: 3.0 mol dm^{-3} KOH + 0.6 mol dm^{-3} H_2O_2 at a flow rate of 80 cm^3 min^{-1}. Operation temperature: room temperature.

voltage and power density against current density. The cell was operated at room temperature with 0.6 mol dm^{-3} H_2O_2 feeding to the cathode compartment. The cell exhibited an open circuit voltage of around 1.5 V. With the increase of current density, the cell voltage decayed almost linearly until reaching to the mass transport control region and then dropped rapidly. This behavior indicated that the cell performance is limited by the poor mass transport within the cathode and the large ohmic resistance from the cathode and the ion transportation through the membrane and the electrolyte. A peak power density of 170 mW cm^{-2} was obtained at 170 mA cm^{-2} and 1.0 V. This performance is comparable with that of Al–H_2O_2 semi-fuel cell using nanoparticle Co_3O_4 cathode [15], but is better than Al–O_2 semi-fuel cell reported by Rota et al. [34]. They found that the single bipolar unit cell of Al–O_2 using alkaline electrolyte had an open circuit voltage of 1.85 V and delivered a maximum power density of about 75 mW cm^{-2} at 0.7 V. High power density can be achieved for Al–H_2O_2 semi-fuel cell by using high concentration of H_2O_2 at the cathode, but at the expense of H_2O_2 utilization efficiency due to the increased chemical decomposition rate of H_2O_2 at high concentration. It is worth to emphasize that $La_{1-x}Sr_xMnO_3$ can also be used as cathode catalysts for other types of fuel cells using H_2O_2 as oxidant, e.g. direct alkaline $NaBH_4$–H_2O_2 fuel cells and direct alcohol–hydrogen peroxide fuel cell. An added advantage of $La_{1-x}Sr_xMnO_3$ cathode is its less sensitivity to the presence of alcohol fuel than noble metal catalysts, such as Pt [30].

4. Conclusions

Perovskite-type $La_{1-x}Sr_xMnO_3$ compounds were synthesized by a sol–gel method using Chitosan as the gelling agent. Their catalytic activities for H_2O_2 electroreduction in alkaline medium were evaluated at room temperature. Dependence of catalytic activity upon the atomic ratio of La to Sr in the $La_{1-x}Sr_xMnO_3$ was found and $La_{0.4}Sr_{0.6}MnO_3$ exhibited the highest activity. Considering rare-earth metals and transition metals are more abundant and cheaper than platinum and other precious materials, perovskite-type $La_{1-x}Sr_xMnO_3$ is an attractive material as electrocatalysts. The Al–H_2O_2 fuel cell using $La_{0.4}Sr_{0.6}MnO_3$ as cathode catalyst displayed an open circuit voltage of 1.5 V and a peak power density of 170 mW cm^{-2}.

Acknowledgements

We gratefully acknowledge the financial support of this research by National Nature Science Foundation of China (20973048), Heilongjiang Provincial Natural Science Foundation (ZJG2007-06-02), Harbin Science and Technology Fund for Young Scholars (2007RFQXG023), and Key Laboratory of Superlight Materials and Surface Technology of Ministry of Education.

References

[1] C. Ponce de Leon, F.C. Walsh, C.J. Patrissi, M.G. Medeiros, R.R. Bessette, R.W. Reeve, J.B. Lakeman, A. Rose, D. Browning, Electrochem. Commun. 10 (2008) 1610–1613.
[2] G.H. Miley, N. Luo, J. Mather, R. Burton, G. Hawkins, L. Gu, E. Byrd, R. Gimlin, P.J. Shrestha, G. Benavides, J. Laystrom, D. Carroll, J. Power Sources 165 (2007) 509–516.
[3] C.P. de Leon, F.C. Walsh, A. Rose, J.B. Lakeman, D.J. Browning, R.W. Reeve, J. Power Sources 164 (2007) 441–448.
[4] R.K. Raman, S.K. Prashant, A.K. Shukla, J. Power Sources 162 (2006) 1073–1076.
[5] R.K. Raman, N.A. Choudhury, A.K. Shukla, Electrochem, Solid State Lett. 7 (2004) A488–A491.
[6] D. Cao, D. Chen, J. Lan, G. Wang, J. Power Sources 190 (2009) 346–350.
[7] L. Gu, N. Luo, G.H. Miley, J. Power Sources 173 (2007) 77–85.
[8] O. Hasvold, N.J. Storkersen, S. Forseth, T. Lian, J. Power Sources 162 (2006) 935.
[9] Hasvold, K.H.a. Johansen, O. Mollestad, S. Forseth, N. St kersen, J. Power Sources 80 (1999) 254–260.
[10] M.G. Medeiros, R.R. Bessette, C.M. Deschenes, C.J. Patrissi, L.G. Carreiro, S.P. Tucker, D.W. Atwater, J. Power Sources 136 (2004) 226–231.
[11] M.G. Medeiros, R.R. Bessette, C.M. Deschenes, D.W. Atwater, J. Power Sources 96 (2001) 236–239.
[12] R.R. Bessette, M.G. Medeiros, C.J. Patrissi, C.M. Deschenes, C.N. LaFratta, J. Power Sources 96 (2001) 240–244.
[13] R.R. Bessette, J.M. Cichon, D.W. Dischert, E.G. Dow, J. Power Sources 80 (1999) 248–253.
[14] J.P. Charles, R.B. Russell, K.K. Yong, R.S. Christian, J. Electrochem. Soc. 155 (2008) B558–B562.
[15] D. Cao, J. Chao, L. Sun, G. Wang, J. Power Sources 179 (2008) 87–91.
[16] W. Yang, S. Yang, W. Sun, G. Sun, Q. Xin, Electrochim. Acta 52 (2006) 9–14.
[17] W. Yang, S. Yang, W. Sun, G. Sun, Q. Xin, J. Power Sources 160 (2006) 1420–1424.
[18] H.B. Urbach, R.J. Bowen, J. Electrochem. Soc. 117 (1970) 1594–1600.
[19] W. Sung, J.-W. Choi, J. Power Sources 172 (2007) 198–208.
[20] D.N. Prater, J.J. Rusek, Appl. Energy 74 (2003) 135–140.
[21] B. Tartakovsky, S.R. Guiot, Biotechnol. Prog. 22 (2006) 241–246.
[22] A. Pizzariello, M. Stred'ansky, S. Miertus, Bioelectrochemistry 56 (2002) 99–105.
[23] D. Cao, L. Sun, G. Wang, Y. Lv, M. Zhang, J. Electroanal. Chem. 621 (2008) 31–37.
[24] H. Liu, L. Zhang, J. Zhang, D. Ghosh, J. Jung, B.W. Downing, E. Whittemore, J. Power Sources 161 (2006) 743–752.
[25] R.K. Raman, A.K. Shukla, J. Appl. Electrochem. 35 (2005) 1157–1161.
[26] V.L.N. Dias, E.N. Fernandes, L.M.S. da Silva, E.P. Marques, J. Zhang, A.L.B. Marques, J. Power Sources 142 (2005) 10–17.
[27] G. Wang, D. Cao, C. Yin, Y. Gao, J. Yin, L. Cheng, Chem. Mater. 21 (2009) 5112–5118.
[28] S.J. Skinner, Int. J. Inorg. Mater. 3 (2001) 113–121.
[29] J. Tulloch, S.W. Donne, J. Power Sources 188 (2009) 359–366.
[30] K. Miyazaki, N. Sugimura, K. Matsuoka, Y. Iriyama, T. Abe, M. Matsuoka, Z. Ogumi, J. Power Sources 178 (2008) 683–686.
[31] P.-Z. Hong, S.-D. Li, C.-Y. Ou, C.-P. Li, L. Yang, C.-H. Zhang, J. Appl. Polym. Sci. 105 (2007) 547–551.
[32] M. Gaudon, C. Laberty-Robert, F. Ansart, L. Dessemond, P. Stevens, J. Power Sources 133 (2004) 214–222.
[33] M. Gaudon, C. Laberty-Robert, F. Ansart, P. Stevens, A. Rousset, Solid State Sci. 4 (2002) 125–133.
[34] M. Rota, C. Comninellis, S. Muller, F. Holzer, O. Haas, J. Appl. Electrochem. 25 (1995) 114–121.